

# Modeling Longshore Sediment Transport for Sustainable Coastal Management in the Damietta Port Area

✉ Ahmed S. A. Ibrahim, ✉ Anas M. El Molla, ✉ Hany G. I. Ahmed

Al-Azhar University, Department of Civil Engineering, Cairo, Egypt

## Abstract

Within the framework of constructing mega coastal ports in Egypt, this research aims to achieve coastal management sustainability in its surroundings by modeling the Longshore Sediment Transport "LST". The literature in the fields of modeling and sediment transport was reviewed and scrutinized. The model was calibrated by contrasting the calculated wave data against 2003 measured data at the Damietta Buoy. The model inputs were tuned to produce a result that was similar to the observed data. Moreover, the model results were validated against 2005 measured data at the Damietta Buoy. Likewise, MIKE21 SM was used to estimate 2011 bed levels within Damietta Port, where 2010 bathymetrical survey data were used. Confident with the model results, it was employed to synthesize transport data for 1940-2020 in terms of LST, Gross LST "GLST" and Net LST "NLST" while considering human intervention and implementing ERA5 wave data. Results were obtained and analyzed, and there was a significant correlation between the significant wave height "Hs" and the wave period "Tp" and GLST (i.e.  $R=0.91-0.79$ , respectively). The analyzed trend results highlighted that in the pre-construction phase of Damietta Port, increases in GLST and NLST were modest (1139.9 and 243.7 m<sup>3</sup>/year, respectively). However, in the post-construction phase of Damietta Port, they escalated between 4679.47 and 3962 m<sup>3</sup>/year. The analyzed results indicated that after introducing coastal protection, GLST and NLST decreased to 2978.1 and 2176 m<sup>3</sup>/year, respectively.

**Keywords:** Damietta port, wave, sediment transport, trend analysis, MIKE21

## 1. Introduction

Coastal regions in the Mediterranean are susceptible to changes in climate. In addition, human intervention amplifies ecosystem vulnerability. However, Egypt is on track to construct mega ports such as Damietta Port. Historically, Damietta Port was constructed in 1982, when two western and eastern jetties were constructed to align its entrance. Additionally, in 2003, breakwaters were constructed within its vicinity. Moreover, from 2016 to 2019, protection was constructed that consists of four T-detached breakwaters.

Accordingly, the literature within the domain of coastal modeling was assembled. Many researchers have investigated this field. Prasad and Kumar [1] documented that the interaction between sea and land is affected by climate change susceptibilities. Likewise, Satterthwaite [2] stated that coastal areas attracted interest because of human development, resulting in population increase

and susceptibility to climate threats (i.e. sea-level-rise, wave activity and erosion). Such threats are impaired by human activities [3-6]. The Mediterranean zone is prone to an accelerated temperature increase that amplifies the coastal erosion risks [7-9]. On the other hand, Khalifa [10] documented that Longshore Sediment Transport "LST" plays a significant role in shoreline morphology, where it is induced by waves. Moreover, Aucan [11] stated that climate change affects localized regions in terms of hydrodynamic phenomena.

Numerical models are vital tools for predicting risky wave events [12,13]. However, these tools require development and validation to promote their reliability, and many studies have introduced many approaches for this purpose [14-16]. On the other hand, Başaran et al. [17] indicated that sustainable coastal management is of global significance, as coastal regions account for approximately 75% of the



**Address for Correspondence:** Ahmed S.A. Ibrahim, Al-Azhar University, Department of Civil Engineering, Cairo, Egypt  
**E-mail:** ahmedsayed.90@azhar.edu.eg  
**ORCID ID:** orcid.org/0009-0005-4402-9889

**Received:** 09.11.2023

**Last Revision Received:** 27.02.2024

**Accepted:** 08.03.2024

**To cite this article:** A. S. A. Ibrahim, A. M. El Molla, and H. G. I. Ahmed, "Modeling Longshore Sediment Transport for Sustainable Coastal Management in the Damietta Port Area." *Journal of ETA Maritime Science*, vol. 12(2), pp. 116-127, 2024.



Copyright © 2024 the Author. Published by Galenos Publishing House on behalf of UCTEA Chamber of Marine Engineers. This is an open access article under the Creative Commons AttributionNonCommercial 4.0 International (CC BY-NC 4.0) License.

Earth's surface. Moreover, they further documented that human activities and climate change transformed the dynamics in coastal zones, which provoked substantial changes in spatial and temporal coastal ecosystems.

Moreover, based on the scrutinized literature, it was obvious that many researchers are delving into LST mechanisms and coastal morphology, whereas Amarouche et al. [18] emphasized that a proper understanding of LST is a prerequisite to effectively manage coastal zones. Likewise, Simav et al. [19] highlighted that the Mediterranean is affected by increasingly human interventions. Focused on the Egyptian coast to offer coastal engineers key factors to effectively manage it [20]. Moreover, Van Rijn et al. [21] suggested that coastal engineers are confronted with a formidable challenge in achieving an accurate prediction of critical factors (i.e. near-shore waves). However, Keshtpoor et al. [22] concentrated on achieving hydrodynamic simulations, LST, and morphological changes, which are imperative for coastal management and planning.

Based on the aforementioned literature, it is important to achieve coastal management sustainability in the vicinity of mega coastal ports in Egypt (i.e., Damietta Port) by modeling the LST, where an 81-year data span was implemented in the present study (i.e. 1940 to 2020 ECMWF-ERA 5 wave data) to consider the long-term impact of climate change and human interventions.

## 2. Methods and Data

### 2.1. Study Area Description

The assembled data were analyzed, from which a clear study area description was perceived and presented. Damietta Port is located in the Nile Delta. It was constructed in 1982. It has a 15-m deep navigation channel. It has two jetties (i.e. eastern and western), and the western jetty is 7.9 km long [23]. The study area stretches over 10 km in the vicinity of Damietta Port, which is a significant maritime project that was initiated in 1981 [24]. Its location was selected because

of its resilience to waves, where coastal accretion was historically documented [25,26].

The study area is distinguished by its very low tidal range (i.e. 14 cm) with a daily fluctuation of 0.60 m [27]. In addition, the grain size “ $D_{50}$ ” of the study area is 0.25 mm and the seabed sediments are 0.11 mm, at depths less than 6 m [28]. However, many defensive measures have been constructed to protect Damietta Port [29]. Among them, for example, are four T-detached breakwaters that were constructed to protect Damietta Port's eastern side. They were established between 2016 and 2019. They extend over 1.5 km. These defensive structures altered the wave reflection pattern, erosion, and accretion along the coast, as shown in Figure 1.

### 2.2. Data Collection

The assembled data encompassed 2003 and 2005 wave data at Damietta Buoy (i.e. located at a depth of 12 m at coordinates of  $31.51^\circ$  N and  $31.76^\circ$  E), as presented in Figure 1. The time series wave data were recorded at 4-h intervals and were obtained from the Egyptian Coastal Research Institute (CoRI). In addition, the ERA5 dataset provides significant data (i.e. wind and waves). Additionally, the available data incorporated 2010 and 2011 bathymetrical data as a set of profiles upstream and downstream of Damietta Port. These bathymetrical data were acquired from CoRI, as shown in Figure 2. Moreover, the data also included wave data from 1940 to 2020 acquired from ERA5. ERA5 data were accessed from <https://cds.climate.copernicus.eu/cdsapp#!/dataset/reanalysis-era5-single-levels?tab=form> [30]. The ERA5 dataset was developed by the European Centre for Medium-Range Weather Forecasts “ECMWF”. It is a reanalysis dataset that provides comprehensive atmospheric and oceanographic information. It encompasses a huge observation array with satellite and buoy readings. ERA5 is renowned for its accuracy. Its resolution is 1 h, while its spatial resolution is  $0.25^\circ$  (i.e. 30 km). The duration of the ERA5 data (81 years) is considered appropriate in considering

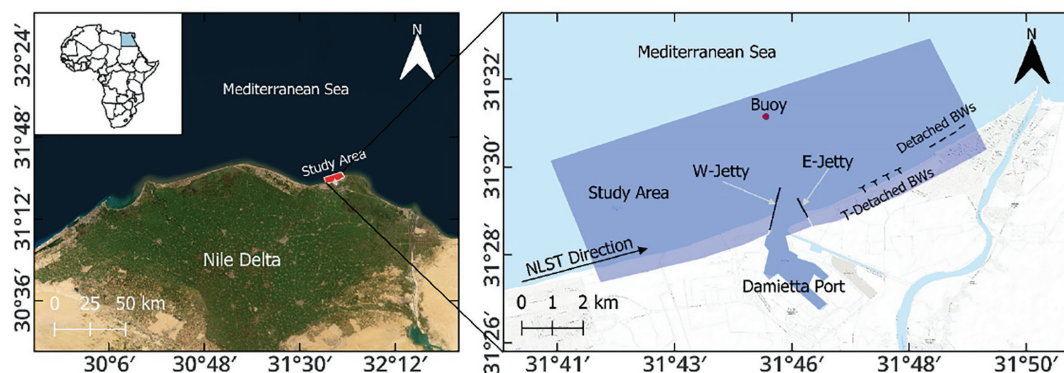


**Figure 1.** Study area with defensive structures and Damietta Buoy location

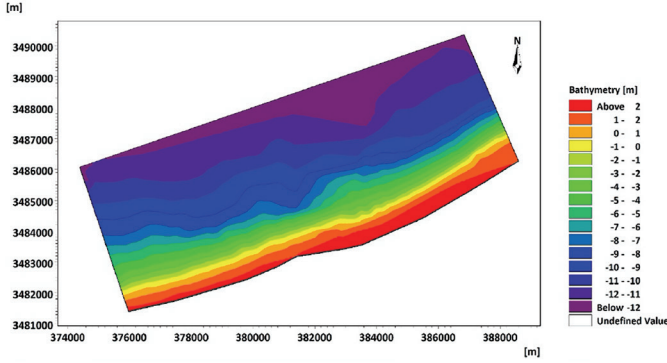


Figure 2. 2010 bathymetric survey of the study area

the recommendations of both the World Meteorological Organisation “WMO” and the Intergovernmental Panel on Climate Change “IPCC”. The World Meteorological Organization recommends investigating climate change using 30-year data [31]. The IPCC recommends using longer datasets to study coastal stability [32]. Unfortunately, the study suffered from a lack of observational data, particularly bathymetric and wave data. The observed wave data were only available for two years (i.e. 2003-2005). Furthermore, bathymetric data for the study area were only available in 2010 and 2011.

### 2.3. Numerical Simulation

MIKE21 was selected for implementation because it is widely accepted and has proven its reliability in many engineering projects. MIKE21 was developed by the Danish Hydraulic Institute “DHI”. It addresses complex morphologies. It performs littoral drift simulations while updating the shoreline morphology [33]. The software encompasses four modules. These are spectral wave “SW” (i.e. MIKE21 SW), hydrodynamic “HD” (i.e. MIKE21 HD), sand transport “ST” (i.e. MIKE21 ST), and shoreline morphology “SM” (i.e. MIKE21 SM) [34].

This section provides a synopsis of the MIKE 21 theoretical background and governing equations.

#### 2.3.1. MIKE21 Governing equations and theoretical background

The governing equations of MIKE21 are the mass equation, momentum equation, salinity, and temperature [35].

Theoretically, MIKE21 SW is a two-dimensional (2-D) wave model [36]. It uses the finite-volume technique on a computational mesh, where differential equations govern the wave dynamics [37,38]. The equations are expressed as follows:

$$\frac{S}{\sigma} = \frac{\partial N}{\partial t} + \nabla(\vec{v}N) \quad (1)$$

Where:

t: time;

v : wave group velocity in the four-dimensional (4-D) phase space formed by x, y,  $\sigma$  and  $\theta$  ( $c_{\sigma}, c_{\theta}, c_x, c_y$ )

$\vec{x}$ : Cartesian coordinates (x,y)

$\sigma$ : relative angular frequency

$\theta$ : direction of wave propagation

$N(\sigma, \theta, x, t)$ : action-density

$\nabla$ : 4-D differential operator (v,  $\sigma$  and  $\theta$ )

S: wave energy source

Principally, MIKE21 HD satisfies the Boussinesq assumptions for hydrostatic pressure. It is based on the incompressible Reynolds-averaged Navier-Stokes equations. It encompasses continuity and momentum equations [35]. Moreover, the 3D hydrodynamic equation can be simplified to a 2D shallow water long wave by time variation by integrating the water depth. MIKE21 HD solves the continuity and momentum equations described as follows:

**Continuity equation:**

$$\frac{\partial h}{\partial t} + \frac{\partial h\bar{u}}{\partial x} + \frac{\partial h\bar{v}}{\partial y} = hS \quad (2)$$

**Momentum equation:**

$$\begin{aligned} \frac{\partial h\bar{u}}{\partial t} + \frac{\partial h\bar{u}^2}{\partial x} + \frac{\partial h\bar{v}\bar{u}}{\partial y} &= f\bar{v}h - gh \frac{\partial \eta}{\partial x} - \frac{h}{\rho_o} \frac{\partial P_a}{\partial x} - \frac{gh^2}{2\rho_o} \frac{\partial \rho}{\partial x} \\ &+ \frac{\tau_{sx}}{\rho_o} - \frac{\tau_{bx}}{\rho_o} - \frac{1}{\rho_o} \left( \frac{\partial S_{xx}}{\partial x} + \frac{\partial S_{xy}}{\partial y} \right) + \frac{\partial}{\partial x} (hT_{xx}) \\ &+ \frac{\partial}{\partial x} (hT_{xy}) + hu_s S \end{aligned} \quad (3)$$

$$\begin{aligned} \frac{\partial h\bar{v}}{\partial t} + \frac{\partial h\bar{v}^2}{\partial y} + \frac{\partial h\bar{v}\bar{u}}{\partial x} &= f\bar{u}h - gh \frac{\partial \eta}{\partial y} - \frac{h}{\rho_o} \frac{\partial P_a}{\partial y} - \frac{gh^2}{2\rho_o} \frac{\partial \rho}{\partial y} \\ &+ \frac{\tau_{sy}}{\rho_o} - \frac{\tau_{by}}{\rho_o} - \frac{1}{\rho_o} \left( \frac{\partial S_{yx}}{\partial x} + \frac{\partial S_{yy}}{\partial y} \right) + \frac{\partial}{\partial y} (hT_{xy}) \\ &+ \frac{\partial}{\partial y} (hT_{yy}) + hv_s S \end{aligned} \quad (4)$$

Where:

t: Time

x, y, and z: Cartesian coordinates

$\eta$ : Surface elevation

d: Still water depth

h: Total water depth ( $\eta + d$ )

u, v, and w: x, y, and z velocity components

f: Coriolis parameter ( $f = 2\Omega \sin\phi$ )

$\Omega$ : angular rate of revolution

$\emptyset$ : geographic latitude  
 $g$ : Acceleration due to gravity  
 $\rho$ : Water density  
 $S_{xx}$ ,  $S_{xy}$ ,  $S_{yx}$ , and  $S_{yy}$ : radiation stress tensor components  
 $P_a$ : atmospheric pressure  
 $\rho_0$ : water reference density  
 $\tau_{sx}$  and  $\tau_{sv}$ : surface wind stresses  
 $\tau_{bx}$  and  $\tau_{bv}$ : bottom stresses  
 $T_{xx}$ ,  $T_{xy}$ , and  $T_w$ : lateral stresses  
 $S$ : point source discharge  
 $u_s$ ,  $v_s$ : water velocity discharged into ambient water.

Theoretically, MIKE21 ST calculates sediment transport while considering wave-current interaction, turbulence, flow velocity, and sediment concentration. It calculates bed load as suspended load by using Shields parameter as flow velocities. It uses a diffusion equation to consider the sediment concentration and vertical fluctuations. Its output provides littoral drift gradients that influence the morphology. Academically, MIKE21 SM utilizes the shoreline continuity equation, where it employs the one-line theory, which divides the shore segment into wedges perpendicular to the shoreline to calculate its position by considering the volumetric sediment changes within each wedge [39].

$$\frac{\Delta N}{\Delta t} = \frac{vol}{dA_z} \quad (5)$$

where:

$\Delta N$ : horizontal shoreline changes

$dA_z$ : vertical closure area

$vol$ : is the sediment volume coming in and out of the wedge

$\Delta t$  denotes the time step.

### 2.3.2. MIKE21 input data

Damietta Port was discretize to initiate the computation, where the computational mesh was defined. It is defined by the UTM coordinates. Its cross-shore and long-shore dimensions are 4.9 km and 13.1 km, respectively. The mesh encompassed the study area and extended seawards to -13.5 m, where the maximum elemental area was 600 m<sup>2</sup> specified near-shore and 3000 m<sup>2</sup> offshore, as shown in Figure 3. The mesh encompassed 48774 triangular elements and 96726 points. MIKE21 input data encompassed ERA5 wave data and bathymetrical data. MIKE 21 SW was operated, where the JONSWAP formulation was employed. MIKE21 SM input data encompass a baseline, an initial shoreline, an edge map, and predefined coastal profiles. The baseline and edge maps define the spatial domain for MIKE21 SM calculations. Regarding the initial shoreline and predefined coastal

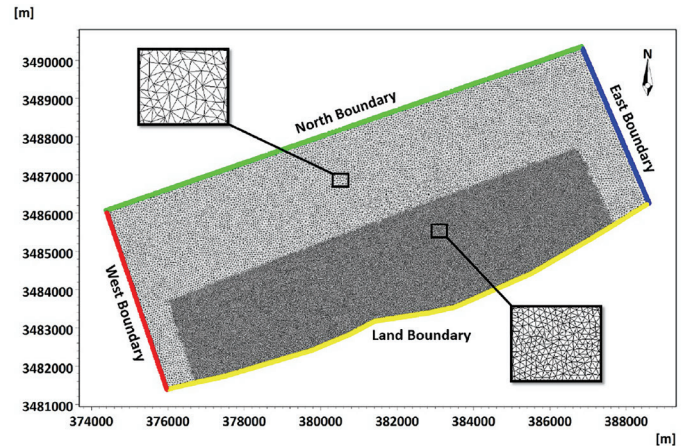


Figure 3. Discretized study area and computational mesh

profiles, they define the bathymetry inside this domain [34]. However, the baseline orientation specifies the direction of shoreline movement, while the initial shoreline defines the initial position prone to accretion or erosion. The baseline and initial shoreline are polylines with nodes with x coordinates. The baseline node spacing designates the resolution of the initial shoreline, where the nodal spacing is 100 m. The edge map divides the shore face into strips perpendicular to the baseline. The offshore boundary of the edge map is the closure depth (i.e. -7.0 m). Changes in sediment volume move the shoreline edge during the simulation. MIKE21 SM calculates the total sediment volume change in a strip by integrating sediment volume change in all mesh elements.

### 2.3.3. Model calibration and validation

Implemented modules MIKE21 SW and MIKE21 SM were calibrated and validated. The main objective is to find the optimal dissipation coefficients (i.e., wave-breaking factors ( $\gamma$  and  $\alpha$ ) and bottom friction) that best fit the model results with the observed data. Accurate estimation of wave energy dissipation is crucial for oceanography and wave modeling to predict wave behavior [40].

To calibrate the MIKE21 model, several simulations were run. Each iteration of the trial-and-error procedure-modified specific critical coefficients. where calibration is based on measurements taken in the study area (e.g., 2003 wave data and 2011 bathymetric data). During the calibration process, the model's performance was assessed using statistical metrics (i.e. bias, Root Mean Square Error "RMSE", Scatter Index "SI" and Correlation Coefficient "CC"). Bias designates the difference between the calculated model results and the measured values. The process reduces errors such as RMSE, bias, and SI across all simulation results. This was achieved using the following set of equations:

$$\bar{x} = \frac{1}{n} \sum_{i=1}^n x \quad (6)$$

$$CC = \frac{\sum_{i=1}^n (x_i - \bar{x})(y_i - \bar{y})}{\sqrt{\sum_{i=1}^n (x_i - \bar{x})^2 \sum_{i=1}^n (y_i - \bar{y})^2}} \quad (7)$$

$$RMSE = \sqrt{\frac{1}{n} \sum_{i=1}^n (y - x)^2} \quad (8)$$

$$BIAS = \frac{1}{n} \sum_{i=1}^n (y - \bar{x}) \quad (9)$$

$$SI = \frac{\sqrt{\frac{1}{n} \sum_{i=1}^n (y - x - BIAS)^2}}{\frac{1}{n} \sum_{i=1}^n |x_i|} \quad (10)$$

Where:

$n$ : number of data

$x$ : measured value

$y$ : estimated or calculated value

### MIKE21 SW

MIKE21 The SW was *calibrated*, where 2003 ERA5 wave data were introduced to it and the wave data at Damietta buoy values were obtained. The simulated wave data listed in the calibration and validation process are computed for the point nearest to the buoy. This was achieved by contrasting the calculated wave data against 2003 measured data at the Damietta Buoy. Based on the calibration process, the model results (i.e.,  $H_s$  and  $T_p$ ) were tuned to produce analogous data. Moreover, the model results were *validated* against 2005 measured data at the Damietta Buoy.

### MIKE21 SM

Similarly, MIKE21 SM was used to provide 2011 bed levels in the vicinity of Damietta Port, where 2010 bathymetrical data was used as an initial condition. MIKE21 SM was calibrated by comparing its calculated bed level data against 2011 measured data at Damietta. Four profiles from 2010 were used (i.e., 2 at port Upstream “US” and 2 at port Downstream “DS”). MIKE 21 was operated, and 2011 profiles were obtained. MIKE21 SM was calibrated by comparing the calculated profiles with the 2011 measured profiles. The model inputs were tuned to produce equivalent levels. Moreover, the model results were validated against another 4 profiles (2 at the US and the other 2 are at the DS).

#### 2.3.4. Long-term simulation

Confident with the calibration and validation process results, MIKE21 was implemented to simulate the study area for a long-time span of 81 years (i.e. 1940-2020), where 1940-2020 ERA5 wave data were implemented

and all human interventions were considered according to their construction time (i.e. western and eastern jetties were constructed in 1982, while the 4 breakwaters were established in 2003 and the T-detached breakwaters were constructed during 2016-2019). Consequently, MIKE21 was run and LST, GLST, and NLST were obtained

## 3. Results and Discussion

Results were obtained and analyzed, from which LST yearly trends were identified. Such trends are fundamental data for further analysis and should be employed in establishing effective development strategies for coastal management. A linear regression equation was used to analyze LST long-term trends, where this relation is described as follows:

$$y = a + b * x \quad (11)$$

Where:

$y$ : meteorological variable

$x$ : time

$a$  and  $b$ : regression coefficients (i.e. obtained from the least square method).

### 3.1. Results Analysis and Discussion of the Calibration and Validation

The results of the calibration and validation processes were analyzed. The analyzed results for the calibration process are presented in Table 1, Figure 4, and Figure 5, where Figure 4 and Figure 5 encompass three subfigures: (a), (b), and (c). Table 1 showcases the statistical metrics employed during the model calibration process across different runs. Each run was evaluated using statistical metrics (i.e. CC, RMSE, bias, and SI). The analysis reveals that dissipation coefficients exhibit a limited impact on CC but show significant improvement in reducing bias and RMSE in the simulated results. After analysis, the third model run outperforms the others in all metrics examined. With correlation coefficients of 0.930 for  $H_s$  and 0.994 for bed levels, the third run shows a strong relationship between predicted and observed values.

Furthermore, it has low RMSE values of 0.180 m for  $H_s$  and 0.212 m for bed levels, indicating little difference between predicted and actual values. In addition, the bias values for  $H_s$  (0.030 m) and bed levels (0.054 m) are close to zero, implying unbiased predictions. Furthermore, the scatter index values for  $H_s$  (0.041 m) and bed levels (0.150 m) are low, indicating little variation around the observed values. Overall, the third run outperformed the other runs because of its strong correlation, low RMSE, negligible bias, and limited SI. The calibration values for the third run were a friction coefficient of 0.01 and wave-breaking factors ( $\alpha = 0.95$  and  $\gamma = 0.8$ ). Additionally, Figure 5 depicts Taylor

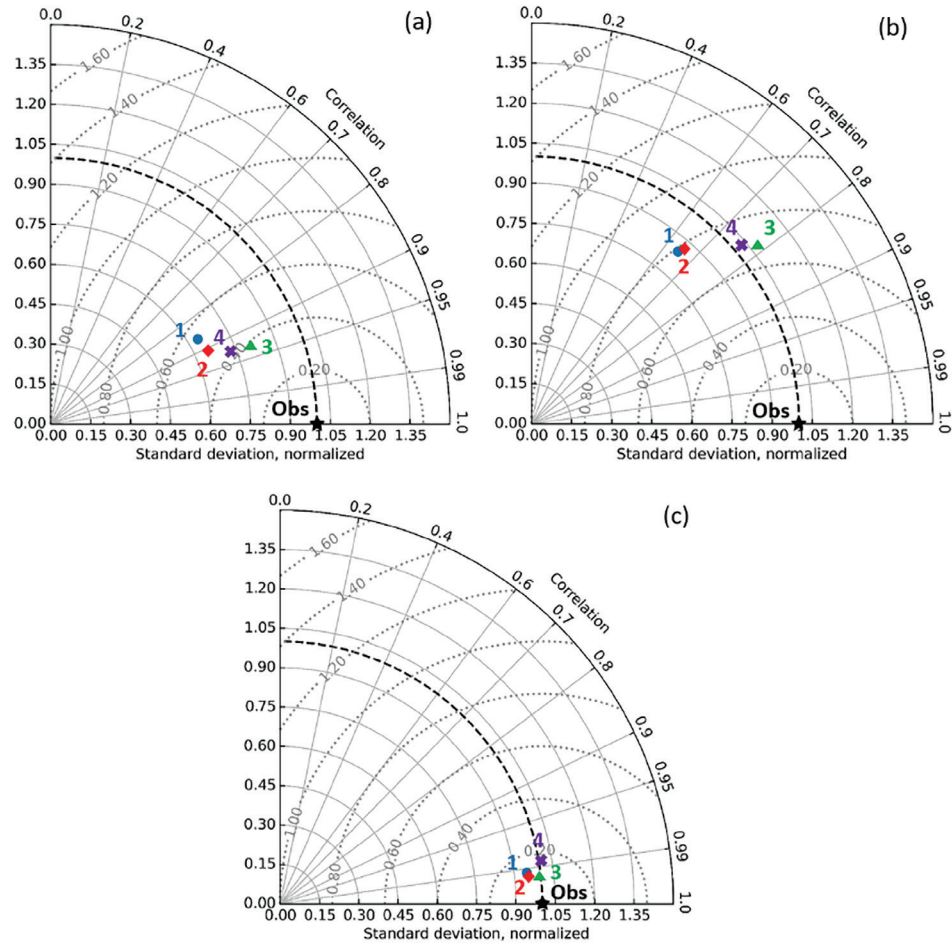


**Figure 4.** The Taylor diagram shows the performances of model runs with different bottom frictions during the calibration process. (a) significant wave height, (b) peak wave period, and (c) bed level

**Table 1.** Statistical metrics for the model calibration process across several runs

Runs	Parameter	CC	RMSE	Bias	SI
1	Significant wave height	0.866	0.250	0.030	0.411
	Peak wave period	0.647	1.213	-0.402	0.172
	Bed level	0.991	0.384	0.287	0.050
2	Significant wave height	0.932	0.184	0.057	0.297
	Peak wave period	0.773	1.090	-0.062	0.163
	Bed level	0.990	0.332	0.248	0.043
3	Significant wave height	0.930	0.180	0.030	0.292
	Peak wave period	0.784	1.040	-0.291	0.150
	Bed level	0.994	0.212	0.054	0.041
4	Significant wave height	0.930	0.191	-0.031	0.312
	Peak wave period	0.771	1.282	-0.814	0.152
	Bed level	0.987	0.324	-0.106	0.061

diagrams of modeled  $H_s$ ,  $T_p$ , and bed levels versus measured values for calibration. Furthermore, Figure 5 contrasts the measured against simulated values (i.e.  $H_s$ ,  $T_p$  and bed levels) for the third run by scatter plots. where the color scale signifies the density of data, and the density of data emphasizes the distribution of observed vs. modeled values. where subfigures (a) and (b) show the calculated and measured values of  $H_s$  and  $T_p$ , respectively, and subfigure (c) shows the bed levels.

The analyzed results for the validation process are presented in Table 2 and Figure 6, where Figure 6 encompasses 3 subfigures (a), (b), and (c). Table 2 lists the statistical metrics (i.e. CC, RMSE, Bias and SI) for the validation process results. From the table, it was obvious that the value of CC was 0.902 for  $H_s$ , while the value of CC for the bed levels was 0.994. Moreover, the table indicates that the RMSE values were low, which signifies a robust agreement between the computed and measured data. However, in certain instances, minor bias was evident, especially for  $H_s$  (i.e. negative bias of

**Table 2.** Statistical metrics related to the calculated and measured values for the validation process

Parameter	CC	RMSE	Bias	SI
Significant wave height	0.902	0.229	-0.032	0.310
Peak wave period	0.723	1.255	-0.186	0.185
Bed level	0.994	0.211	0.095	0.037

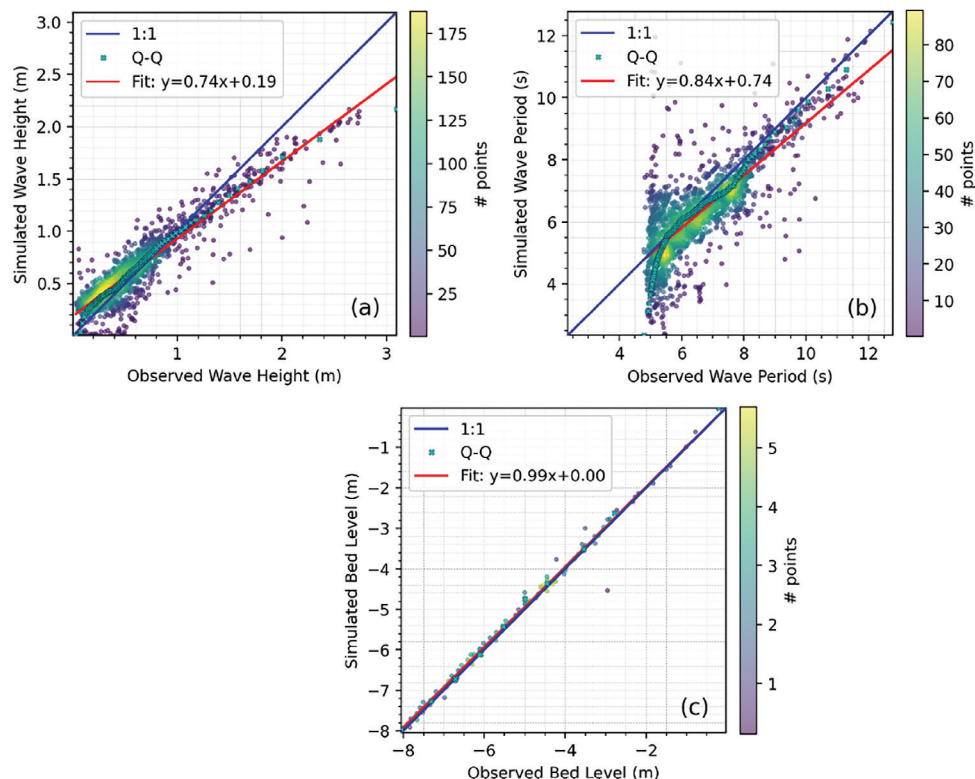


**Figure 5.** Scatter plots for the third model run in the calibration process. (a) significant wave height, (b) peak wave period, and (c) bed level

-0.032). However, the plots presented in Figure 6 provide a visual assessment of the model's performance, emphasizing the agreement between observed and calculated values.

### 3.2. Results Analysis and Discussion of the Wave Climate

Results of the wave climate (i.e.,  $H_s$  and  $T_p$ ) were analyzed and presented in Figure 7, which provides monthly wave data. The figure designates that the  $H_s$  distribution reaches the minimum during the 1<sup>st</sup> quartile, while it attains the average in the 3<sup>rd</sup> quartile. However, the maximum values vary monthly from 1940 to 2020. Moreover, it emphasizes that storms are frequent and intense from February to April. However, the wave statistical distribution varies significantly on a monthly basis.  $H_s$  at 12 m depth indicated its variability within the range of 0.01-4.94 m, whereas  $T_p$  varied within the range of 2-14.3 s, with a mean wave direction of 326°. Moreover, the figure indicates that during winter,  $H_s$  ranged between 0.55 and 1.55 m, with an average of 1.03 m. However,  $T_p$  varies between 5.4 and 8.1 s. In contrast, during summer,  $H_s$  ranges between 0.61 and 1.28 m, whereas  $T_p$  ranges between 4.9 and 7 s. However, in autumn and spring, the mean  $H_s$  was 0.85 m, and the monthly variation in  $H_s$  indicated that the maximum  $H_s$  occurred in November, December, January, February, and March. However,  $H_s$  is less than 1 m throughout the year (i.e. 68% of the time), while  $H_s$  ranges between 1 m and 2

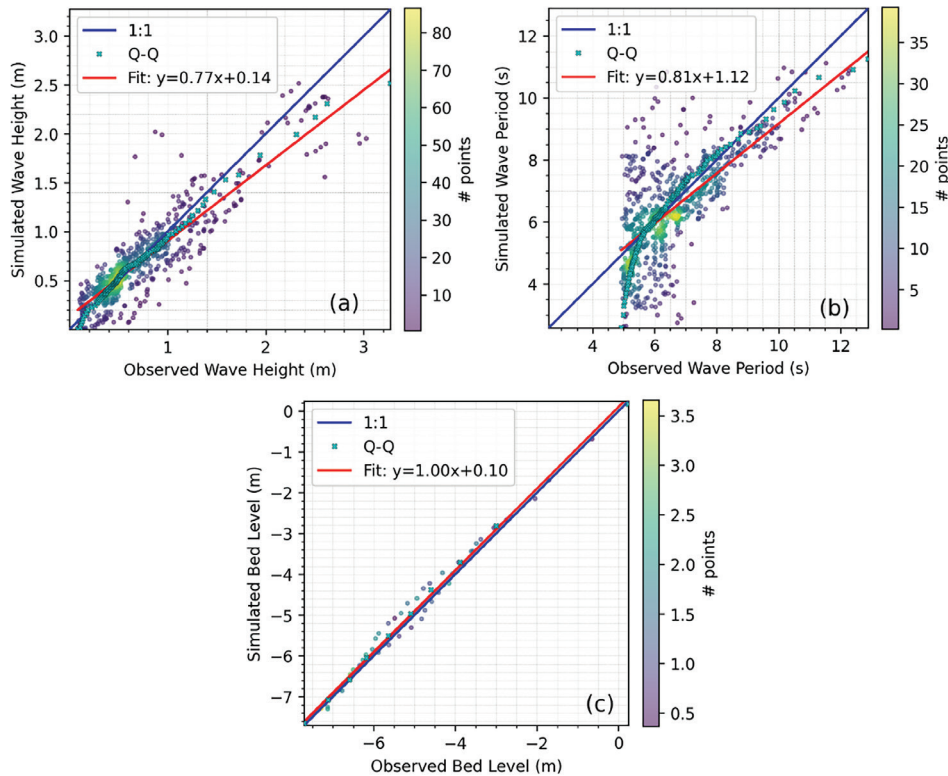


Figure 6. Scatter plots for the validation process: (a) significant wave height, (b) peak wave period, and (c) bed level

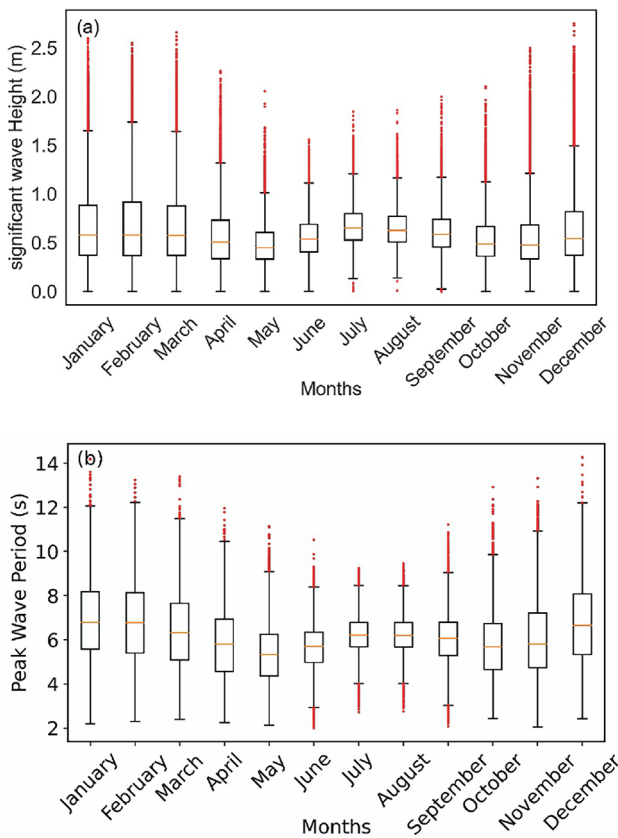


Figure 7. Monthly variations in wave climate during 1940-2020: (a) significant wave height (m) and (b) peak wave period (s)

m during 28% of the year, and  $H_s$  exceeds 2 m only 0.04% of the year. This agrees with [41,42], who documented that the waves predominantly (i.e. 86%) come from the N-NW sector.

Figure 8 depicts the differences in wave height distribution in the study area during the pre-construction and post-construction phases of Damietta Port. During the pre-construction phase (Figure 8a), the wave height distribution reflected the natural conditions of the area. The distribution of the wave heights changed after construction (Figure 8b). However, the existence of these structures modified the wave climate in the area by changing the wave propagation sequences and heights.

### 3.3. Results Analysis and Discussion of Sediment Transport

The results of LST analysis are presented in Figure 9, which indicates that LST varies where the sediment is disturbed by human interventions. In addition, the LST long-term trend was achieved using the best-fit line method.

In the pre-construction phase of Damietta Port, GLST ranged between  $0.87$  and  $1.5 \times 10^6$  m<sup>3</sup>/year, with an average of  $1.1 \times 10^6$  m<sup>3</sup>/year. Likewise, NLST varied between  $0.49$  and  $1.04 \times 10^6$  m<sup>3</sup>/year with an average of  $0.73 \times 10^6$  m<sup>3</sup>/year. Sediment transport values agree with previous findings in the study area, where researchers estimated the transport to be  $0.66 \times 10^6$  m<sup>3</sup>/year to the east and  $0.26 \times 10^6$  m<sup>3</sup>/year

to the west with an NLST of  $0.4 \times 10^6 \text{ m}^3/\text{year}$  to the east [26]. However, other researchers estimated NLST to be  $0.8 \times 10^6 \text{ m}^3/\text{year}$  [43], while Frihy et al. [44] estimated it to be  $0.6\text{--}1.8 \times 10^6 \text{ m}^3/\text{year}$ .

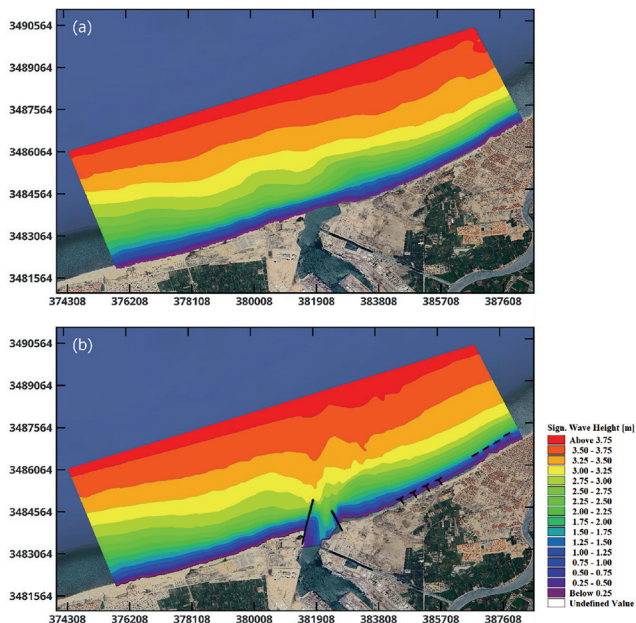


**Figure 8.** Significant wave height distributions for two phases: (a) pre-construction phase of Damietta Port and (b) post-construction phase of Damietta Port and associated protection structures

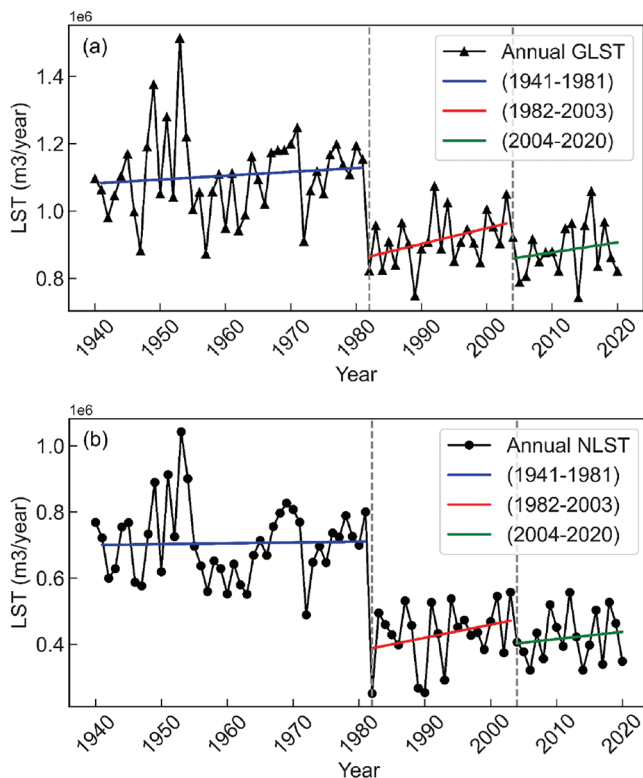


**Figure 9.** Annual LST trend during 1940-2020: (a) annual NLST and (b) annual GLST

In the post-construction phase of Damietta Port, LST experienced a rapid decrease and was trapped within the navigation channel, which eventually obstructed port access.

After implementing the Port structures, GLST fluctuated annually, with the highest GLST recorded in 1992 (i.e.  $1.07 \times 10^6 \text{ m}^3/\text{year}$ ), while the lowest GSR occurred in 1989 (i.e.  $0.75 \times 10^6 \text{ m}^3/\text{year}$ ); (Figure 9a). However, the annual GLST was  $0.9 \times 10^6 \text{ m}^3/\text{year}$ . Furthermore, the NLST varied, where the highest annual NLST was  $0.65 \times 10^6 \text{ m}^3/\text{year}$ . In contrast, the lowest recorded NLST value was  $0.2 \times 10^6$ , with an average value of  $0.42 \times 10^6 \text{ m}^3/\text{year}$  (Figure 9b). A similar estimate has been previously documented. However, Frihy et al. [42] employed fluorescent tracers to designate the annual LST. The study revealed that GLST was  $0.85 \times 10^6 \text{ m}^3/\text{year}$ , while NLST was  $0.49 \times 10^6 \text{ m}^3/\text{year}$ .

To gain insights into annual LST, we used trend lines to represent the average LST values for each year (Figure 9). The analysis reveals significant positive trends in LST, both before and after the construction of Damietta Port and the implementation of coastal protection structures. These trends underscore the dynamic response of LST to human interventions, potentially impacting coastal geomorphology and sediment management strategies. In the pre-construction phase of Damietta Port, both GLST and NLST exhibited relatively modest trends. The trend in GLST showed a positive average of  $1139.9 \text{ m}^3/\text{year}$ , while the trend in NLST was also positive, averaging  $243.7 \text{ m}^3/\text{year}$ .

In the post-construction phase of Damietta Port, there was a substantial increase in both GLST and NLST trends. The trend in GLST significantly increased to  $4679.47 \text{ m}^3/\text{year}$ , and the trend in NLST also experienced a notable increase, reaching  $3962 \text{ m}^3/\text{year}$ . These findings strongly indicate that the Port's construction had a significant impact on LST processes along the coast. From 2004 to 2020, following the implementation of coastal protection structures, there was a noticeable decrease in both GLST and NLST trends. The trend in GLST decreased to  $2978.1 \text{ m}^3/\text{year}$ , and the trend in NLST decreased to  $2176 \text{ m}^3/\text{year}$ . This decline suggests that the coastal protection structure likely played a crucial role in mitigating LST trends and effectively stabilizing sediment dynamics in the area.

### 3.4. Results Analysis and Discussion of Sediment Transport and Wave Climate

Results spanning over eight decades (1940-2020) of LST and wave climate (i.e.  $H_s$  and  $T_p$ ) were obtained in the Damietta buoy location, analyzed, and presented in Figure 10. The analysis revealed strong correlations among these parameters. From the figure, clear was the strong correlation between  $H_s$  and GLST so as NLST, where  $R$  was 0.91; (Figure

10a) and was 0.71; (Figure 10b), respectively. In addition,  $T_p$  had a strong correlation between  $T_p$  and GLST, similar to NLST, where  $R$  was 0.79, as shown in Figure 10c, and 0.66, as shown in Figure 10d.

#### 4. Conclusions and Recommendations

This study represents a substantial advancement in our understanding of the complex interactions among wave climate, LST, and human interventions in coastal regions, with a specific focus on the Damietta area in the Eastern Mediterranean. By analyzing an extensive 81-year dataset, which includes four-hour interval data, the study has provided valuable insights into the coastal dynamics of this region. MIKE 21 SW proved its reliability in transforming waves from offshore to the Damietta buoy. MIKE 21 SM proved its trustworthiness in estimating bed levels in the Damietta area. A better understanding of the complex interaction between waves, LST, and human interventions in coastal regions was obtained. Valuable insights were attained into the coastal dynamics of the Damietta region, where it was clear that waves less than 1 m prevailed 68% of the year and waves exceeding 2 m occurred 0.04% of the time. LST has varied significantly over the years, which indicates the dynamic nature of LST in the Damietta area. NLST migrates eastward;

however, directional reversals were evident. Implementing protection structures for LST dynamics helped reduce impact of Damietta Port by stabilizing sediment processes and reducing GLST and NLST trends.

**Based on the conclusions, the following recommendations were made:**

Implement a robust monitoring system for waves and LST to gain better insights into the complexities of coastal dynamics. Coastal planning should be integrated to consider the interaction between wave climate, sediment dynamics, and human activities. Strike a balance between sediment management and coastal processes. The protection work should be sustainable and compatible with the surrounding ecosystem.

**Based on the suggested recommendations, future research is advised to:**

Investigate temporal wave trends over a shorter time intervals. Conduct a detailed analysis of storm events and their impact on waves and sediment transport. Investigate the socioeconomic impacts of longshore transport on coastal communities. Assess the consequences of changing sediment dynamics on coastal infrastructure. Assess coastal areas' resilience to climate change and human interventions.

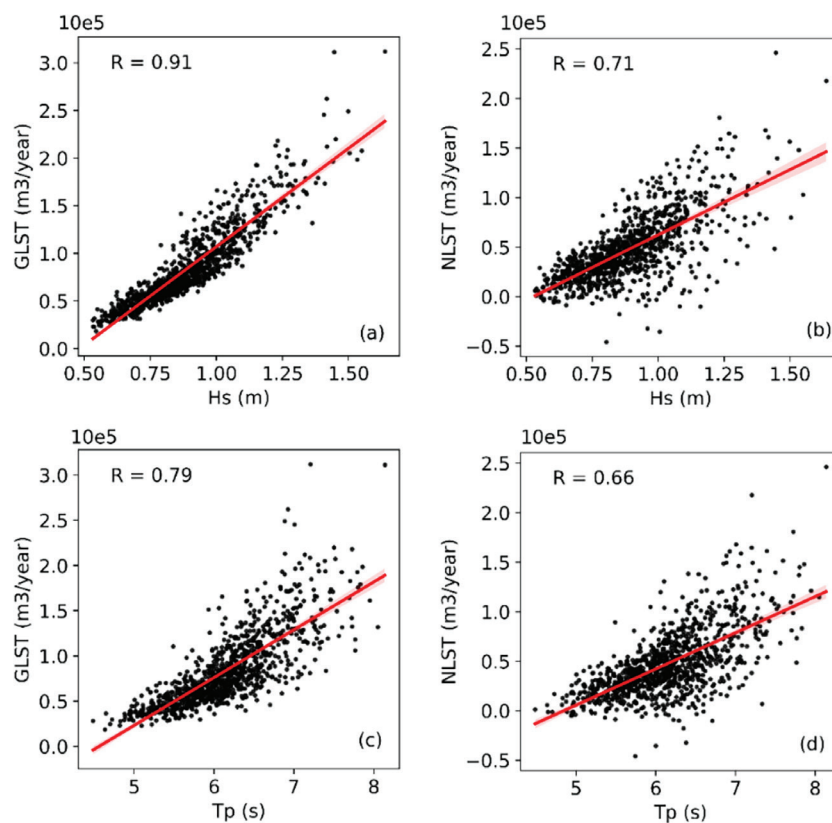


**Figure 10.** Longshore sediment transport (i.e. GLST and NLST) versus wave climate (i.e. Hs,  $T_p$ )

## Authorship Contributions

Concept design: A. S. A. Ibrahim, A. M. El Molla, and H. G. I. Ahmed, Data Collection or Processing: A. S. A. Ibrahim, Analysis or Interpretation: A. S. A. Ibrahim, A. M. El Molla, and H. G. I. Ahmed, Literature Review: A. S. A. Ibrahim, and H. G. I. Ahmed, Writing, Reviewing and Editing: A. S. A. Ibrahim, A. M. El Molla, and H. G. I. Ahmed.

**Funding:** The authors declare that no funding was received for this research, authorship, or publication.

## References

- [1] D. H. Prasad, and N. D. Kumar, "Coastal erosion studies-a review," *International Journal of Geosciences*, vol. 5, pp. 341-345, Mar 2014.
- [2] D. Satterthwaite, "The transition to a predominantly urban world and its underpinnings," *Human Settlements Discussion Paper Series- Theme: Urban Change -4*, pp. 1-91, 2007.
- [3] A. Arns, S. Dangendorf, J. Jensen, S. Talke, J. Bender, and C. Pattiaratchi, "Sea-level rise induced amplification of coastal protection design heights". *Scientific Reports*, vol. 7, pp. 1-9, 2017.
- [4] A. Grases, V. Gracia, M. García-León, J. Lin-Ye, and J. P. Sierra, "Coastal flooding and erosion under a changing climate: Implications at a low-lying coast (Ebro Delta)". *Water (Switzerland)*, vol. 12, 346, Jan 2020.
- [5] R. Almar, et al. "Response of the Bight of Benin (Gulf of Guinea, West Africa) coastline to anthropogenic and natural forcing, Part1: Wave climate variability and impacts on the longshore sediment transport". *Continental Shelf Research*, vol. 110, pp. 48-59, Nov 2015.
- [6] S. Knobler, D. Liberzon, and F. Fedele, "Large waves and navigation hazards of the Eastern Mediterranean Sea". *Scientific Reports*, vol. 12, pp. 1-17, Oct 2022.
- [7] IPCC, "Climate change 2022: impacts, adaptation and vulnerability. Contribution of working group II to the sixth assessment report of the intergovernmental panel on climate change [H.-O. Pörtner, D.C. Roberts, M. Tignor, E.S. Poloczanska, K. Mintenbeck, A. Alegr," Cambridge Univ. Press. Cambridge Univ. Press. Cambridge, UK New York, NY, USA, vol. 3056, 2022.
- [8] A. R. Birben, I. H. Özölçer, S. Karasu, and M. I. Kömürçü, "Investigation of the effects of offshore breakwater parameters on sediment accumulation". *Ocean Engineering*, vol. 34, pp. 284-302, Feb 2007.
- [9] M. R. Nikmanesh, and N. Talebbeydokhti, "Numerical simulation for predicting concentration profiles of cohesive sediments in surf zone". *Scientia Iranica*, vol. 20, pp. 454-465, Jun 2013.
- [10] M. A. Khalifa, "Adoption of recent formulae for sediment transport calculations applied on the Egyptian Nile delta coastal area". *Journal of Coastal Conservation*, vol. 16, pp. 37-49, Oct 2011.
- [11] J. Aucan, "Effects of climate change on sea levels and inundation relevant to the pacific islands what is already happening?". *PACIFIC MARINE CLIMATE CHANGE REPORT CARD, Science Review*, pp. 43-49, 2018.
- [12] K. E. Saraçoğlu, H. A. Arı Güner, C. Şahin, Y. Yüksel, and E. Özkan Çevik, "Evaluation of the wave climate over the black sea: field observations and modeling". In *Proceedings of 35th Conference on Coastal Engineering, Antalya, Turkey, 2016*, pp. 1-8, Jun 2016.
- [13] F. Barbariol, et al. "Wind waves in the mediterranean sea: an ERA5 reanalysis wind-based climatology". *Frontiers in Marine Science*, vol. 8, pp. 1-23, Nov 2021.
- [14] P. G. Remya, R. Kumar, S. Basu, and A. Sarkar, "Wave hindcast experiments in the Indian Ocean using MIKE 21 SW model". *Journal of Earth System Science*, vol. 121, pp. 385-392, May 2012.
- [15] M. H. Moeini, and A. Shahidi, "Application of two numerical models for wave hindcasting in Lake Erie". *Applied Ocean Research*, vol. 29, pp. 137-145, Jul 2007.
- [16] S. Hadadpour, H. Moshfeghi, E. Jabbari, and B. Kamranzad, "Wave hindcasting in Anzali, Caspian Sea: a hybrid approach," *Journal of Coastal Research*, vol. 65, pp. 237-242, Jan 2013.
- [17] B. Başaran, A. Güner, and H. Anil, "Effect of wave climate change on longshore sediment transport in Southwestern Black Sea". *Estuarine, Coastal and Shelf Science*, vol. 258, 107415, Sep 2021.
- [18] K. Amarouche, A. Akpınar, N. E. I. Bachari, R. E. Çakmak, and F. Houma, "Evaluation of a high-resolution wave hindcast model SWAN for the West Mediterranean basin". *Applied Ocean Research*, vol. 84, pp. 225-241, Mar 2019.
- [19] Ö. Simav, D. Z. Şeker, and C. Gazioğlu, "Coastal inundation due to sea level rise and extreme sea state and its potential impacts: Çukurova Delta case". *Turkish Journal of Earth Sciences*, vol. 22, pp. 671-680, 2013.
- [20] J.-L. Chen, T.-J. Hsu, F. Shi, B. Raubenheimer, and S. Elgar, "Hydrodynamic and sediment transport modeling of New River Inlet (NC) under the interaction of tides and waves". *Journal of Geophysical Research: Oceans*, vol. 120, pp. 4028-4047, 2015.
- [21] L. C. V. Rijn, J. S. Ribberink, J. V. D. Werf, and D. J. R. Walstra, "Coastal sediment dynamics: recent advances and future research needs". *Journal of Hydraulic Research*, vol. 51, pp. 475-493, 2013.
- [22] M. Keshtpoor, J. A. Puleo, F. Shi, and N. R. DiCosmo, "Numerical simulation of nearshore hydrodynamics and sediment transport downdrift of a tidal inlet". *Journal of Waterway, Port, Coastal, and Ocean Engineering*, vol. 141, Jul 2014.
- [23] A. M. Khalifa, M. R. Soliman, and A. A. Yassin, "Assessment of a combination between hard structures and sand nourishment eastern of Damietta harbor using numerical modeling". *Alexandria Engineering Journal*, vol. 56, pp. 545-555, Dec 2017.
- [24] ASRT, "Sedimentation in Damietta Harbor; Academy of Scientific Research and Technology Final Report; ASRT: Cairo, Egypt," 1988.
- [25] H. M. El Asmar, and K. White, "Changes in coastal sediment transport processes due to construction of New Damietta Harbour, Nile Delta, Egypt". *Coastal Engineering*, vol. 46, pp. 127-138, Jul 2002.
- [26] M. Sogreah, "Effects on the construction of the Port of Damietta on the evolution of the littoral drift," *Consult. Report, number 35/1202/R9*, p. 35, 1982.
- [27] N. El-Fishawi, "Relative changes in sea level from tide gauge records at Burrulus, central part of the Nile Delta coast," *INQUA MBSS Newsl.*, vol. 16, pp. 53 - 61, 1994.

- [28] F. M. Eid, S. H. S. El-Din, and K. A. A. El-Din, "Sea level variation along the Suez Canal". *Estuarine, Coastal and Shelf Science*, vol. 44, pp. 613-619, May 1997.
- [29] H. M. El-Asmar, M. M. N. Taha, and A. S. El-Sorogy, "Morphodynamic changes as an impact of human intervention at the Ras El-Bar-Damietta Harbor coast, NW Damietta Promontory, Nile Delta, Egypt". *Journal of African Earth Sciences*, vol. 124, pp. 323-339, Dec 2016.
- [30] Hersbach, H. *et al.*, "ERA5 hourly data on single levels from 1940 to present," Copernicus Climate Change Service (C3S) Climate Data Store (CDS) doi: 10.24381/cds.adbb2d47 (accessed on 10 March 2023).
- [31] P. Vethamony, V. M. Aboobacker, K. Sudheesh, M. T. Babu, and K. Ashok Kumar, "Demarcation of inland vessels' limit off Mormugao port region, India: a pilot study for the safety of inland vessels using wave modelling," *Natural Hazards*, vol. 49, pp. 411-420, 2009.
- [32] IPCC, "Climate Change 2013: The Physical Science Basis," *Contrib. Work. Gr. I to Fifth Assess. Rep. Intergov. Panel Clim. Chang.* [Stocker, T.F., D. Qin, G.-K. Plattner, M. Tignor, S.K. Allen, J. Boschung, A. Nauels, Y. Xia, V. Bex P.M. Midgley (eds.)]. Cambridge Unive, p. 1535, 2013.
- [33] A. Seenath, "A new approach for handling complex morphologies in hybrid shoreline evolution models," *Applied Ocean Research*, vol. 141, 103754, Dec 2023.
- [34] DHI, "Introducing the MIKE 21 Shoreline Morphology Module, Denmark, DHI Headquarters," 2017.
- [35] DHI, "MIKE 21 & MIKE 3 Flow Model FM - Hydrodynamic Module, Denmark, DHI Headquarters," 2017.
- [36] DHI, "MIKE 21 Wave Modelling - MIKE 21 Spectral Waves FM, Denmark, DHI Headquarters," 2017.
- [37] G. J. L. Komen, M. Cavaleri, K. Donelan, S. Hasselmann, and P. A. E. M. Janssen, "Dynamics and modelling of ocean waves," *Cambridge University Press*, vol. UK, pp. 560, 1994.
- [38] I. R. Young, "Wind generated ocean waves". *Elsevier*, vol. 2, Apr 1999, [Online]. Available: <https://api.semanticscholar.org/>
- [39] DHI, "MIKE 21 & MIKE 3 Flow Model FM - Sand Transport Module, Denmark, DHI Headquarters," 2017.
- [40] A. Akpınar, and S. Ponce de León, "An assessment of the wind re-analyses in the modelling of an extreme sea state in the Black Sea," *Dynamics of Atmospheres and Oceans*, vol. 73, pp. 61-75, Mar 2016.
- [41] A. Abo Zed, "Effects of waves and currents on the siltation problem of Damietta harbour, Nile Delta coast, Egypt," *Mediterranean Marine Science*, vol. 8, pp. 33-48, 2007.
- [42] O. E. Frihy, A. B. Abd El Moniem, and M. S. Hassan, "Sedimentation processes at the navigation channel of the Damietta Harbour on the Northeastern Nile Delta coast of Egypt". *Journal of Coastal Research*, vol. 18, pp. 459-469, 2002.
- [43] T. Tech., "Shoreline master plan for the Nile Delta coast," *Prog. Rep. number 1*, p. 143, 1984.
- [44] H. M. El-Asmar and K. White, "Rapid updating of maps of dynamic coastal landforms by segmentation of Thematic Mapper imagery, example from the Nile Delta, Egypt," *In Proceedings of 23rd Annual Conference of the Remote Sensing Society, The University of Reading. Remote Sensing Society, Nottingham*, pp. 515-520, 1997.